applied sciences

MDPI

Article

Multi-Criteria Decision-Making Method for Simple and Fast Dimensioning and Selection of Glass Tube Collector Type Based on the Iterative Thermal Resistance Calculation Algorithm with Experimental Validation

Aleksandar Nešović [1], Robert Kowalik [2,*], Dragan Cvetković [1] and Agata Janaszek [2]

[1] Institute for Information Technologies, University of Kragujevac, Jovana Cvijića bb, 34000 Kragujevac, Serbia; aca.nesovic@kg.ac.rs (A.N.); dragan_cw8202@yahoo.com (D.C.)
[2] Faculty of Environmental Engineering, Geodesy and Renewable Energy, Kielce University of Technology, Tysiaclecia P.P. 7, 25-314 Kielce, Poland; ajanaszek@tu.kielce.pl
* Correspondence: rkowalik@tu.kielce.pl

Abstract: This paper presents an analytical method for the dimensioning and selection of the four glass tube collector types: single-glazed with an air layer, single-glazed with a vacuum layer, double-glazed with an air layer, and double-glazed with a vacuum layer. In the first part of the paper (dimensioning phase), the iterative thermal resistance calculation algorithms were developed for all glass tube collector types, whereby the iterative thermal resistance calculation algorithm of the single-glazed tube collector with an air layer was experimentally tested and validated. The second part of the paper (selection phase) uses a multi-criteria decision-making method to determine the optimal glass tube collector design. Unlike other papers, three indicator groups are taken into account in this case: geometric (mass, surface occupation, total surface occupation, volume occupation), economic (manufacturing and exploitation costs), and ecological (embodied energy and greenhouse gas emission). The proposed method is characterized by simple and fast calculations with satisfactory accuracy, which avoids high investment costs (experimental research), approximation and discretization of physical models (numerical research), and a large number of input parameters with boundary conditions (theoretical research). It should be noted that, with certain additions and changes, it can also be applied to other solar thermal collectors, so the authors believe such tools are handy for the global scientific public.

Keywords: air layer; glass tube; multi-criteria decision-making method; absorber plate; solar thermal collector; thermal resistance; vacuum layer

Citation: Nešović, A.; Kowalik, R.; Cvetković, D.; Janaszek, A. Multi-Criteria Decision-Making Method for Simple and Fast Dimensioning and Selection of Glass Tube Collector Type Based on the Iterative Thermal Resistance Calculation Algorithm with Experimental Validation. *Appl. Sci.* **2024**, *14*, 6603. https://doi.org/10.3390/app14156603

Academic Editors: Yuyang Li, Zhenyuan Xu, Zhanjun Cheng and Peng Zhao

Received: 20 June 2024
Revised: 22 July 2024
Accepted: 26 July 2024
Published: 28 July 2024

1. Introduction

Solar technology is constantly developing and is currently expanding. This scientific field includes a large number of different solar constructions, such as solar collectors (SCs), photovoltaic panels (PVs), and hybrid (photovoltaic–thermal) collectors (PVTCs).

Of all SCs, flat-plate collectors (FPCs) and evacuated tube collectors (ETCs) have the greatest practical and commercial applications [1,2] because they are distinguished by a relatively simple manufacturing process, reduced dimensions, satisfactory thermal performance, and relatively low price. In addition, ETCs also offer higher thermal efficiency [3] and working fluid temperature [4] than FPCs, so they can be found almost everywhere: in the residential sector [5], in the commercial (public) sector [6], in the industrial sector [7], etc. In the mentioned sectors, ETCs are used in heating systems [8], cooling systems [9], ventilation systems [10], air conditioning systems [11], hot water systems [12], etc. Some ETC constructions are modified by concentrators [13], reflectors [14], mirrors [15,16], and tracking systems [17–19] accompanied

by a large number of experimental [20], numerical [21], and theoretical (analytical or mathematical) [22] investigations.

The hybrid configuration with ETCs is presented in [23]. The experimental investigation revealed that the solar thermal collector's maximum outlet temperature, efficiency, and maximum cooling capacity were 87 °C, 56%, and 4.6 kW, respectively. In [24], a comparative study was carried out on the performance of an individual SC under laboratory conditions and field conditions (experimental study). A compound parabolic concentrator (CPC) with an ETC has been used to apply boiler feed-water preheating. The performance monitoring and evaluation of the actual installation were carried out over 10 months. The system was designed to supply an average of 448,500 kWh-thermal/year, saving the equivalent amount of fossil fuel. The ETC is developed in [25] to achieve high heating-medium temperature. They used 10 mol% of ethylene glycol in water as the heat transfer fluid. The results showed that the average temperature of the heat transfer fluid in a modified tube increased to 160.32 °C, with an efficiency increase of 34.96%.

Kaya et al. numerically investigated an ETC with a U-tube [26]. The thermal performance of the analyzed SC was simulated for different operating conditions. They used higher thermal conductivity working fluids: Ag, ZnO, and MgO nanoparticles in 30%:70% (by volume) ethylene glycol/pure water mixture and different nanoparticle volumetric concentrations.

For example, a new ETC construction with inner concentrating, which has 10% higher thermal efficiency than classic ETCs, was proposed, fabricated, and presented in [27]. Additionally, the mathematical model of the mentioned solar collector was developed. Ma et al. [28] mathematically considered a double-glazed ETC with a U-tube, where the absorber film is deposited on the outer surface of the absorber tube.

In the review paper presented in [29], Chopra et al. analyzed ETCs with direct flow and heat pipes, providing comprehensive theoretical analysis. The review paper [30] focused on air as a working fluid in ETCs and summarized design configurations and simulation works, using nanofluids and phase change materials to understand their influence on the thermal performance of these ETCs.

The state of the market, along with the available literature, shows that many ETC constructions never progress beyond the case-study phase to the commercial phase. The reasons include complex technological manufacturing procedures, costly experimental investigations, use of scarcely available materials, high manufacturing costs, high final product prices, and difficult transportation (including assembly and maintenance). Some solutions are much larger in terms of surface occupancy and volume occupancy [31] compared to the basic versions of solar collectors—indicators that authors often ignore in their works. Numerical and theoretical investigations intended to describe the functioning principles of such solar installations are further complicated by various problems: approximation and discretization of physical models, selection and description of physical and chemical phenomena, definition of properties of working fluids, determination of specific boundary conditions, and inclusion of a large number of influential parameters, among others. It has been noted that ecological indicators (embodied energy and greenhouse gas emissions) are also often neglected despite their importance for green technology, which is emphasized globally today [32–34].

Due to all of the above, this paper presents a simple and fast analytical method for the dimensioning and selection of glass tube collectors (GTCs) with direct water flow as the working fluid. The simplicity of the method is reflected in the development of a mathematical model for calculating thermal resistance in GTCs (based on an iterative calculation algorithm), regardless of the number and performance of both the glass tubes (GTs) and the interspace. The mathematical model was applied to the following types of GTCs: single-glazed tube collector (SGTC) with an air layer, SGTC with a vacuum layer, double-glazed tube collector (DGTC) with an air layer, and DGTC with a vacuum layer. The mathematical model for the SGTC with an air layer has been experimentally tested and verified using measurement data. Finally, the multi-criteria decision-making (MCDM) method was used

to determine the optimal design of the GTC. This method is rarely used in such studies. For this purpose, four geometric criteria (mass, surface occupancy, total surface occupancy, volume occupancy), two economic criteria (manufacturing costs, exploitation costs), and two ecological criteria (embodied energy, greenhouse gas emissions) were used. The aim of this paper is to highlight the importance of evaluating GTC performance from several different angles. Only then can sustainable development be ensured, as well as energy, economic, and environmental security.

2. Research Area

This section delineates four configurations of glass tube collectors (GTCs) (Figure 1); they are:

- SGTC with air layer (collector type S1);
- SGTC with a vacuum layer (type S2 collector);
- DGTC with air layer (collector type S3);
- DGTC with a vacuum layer (collector type S4).

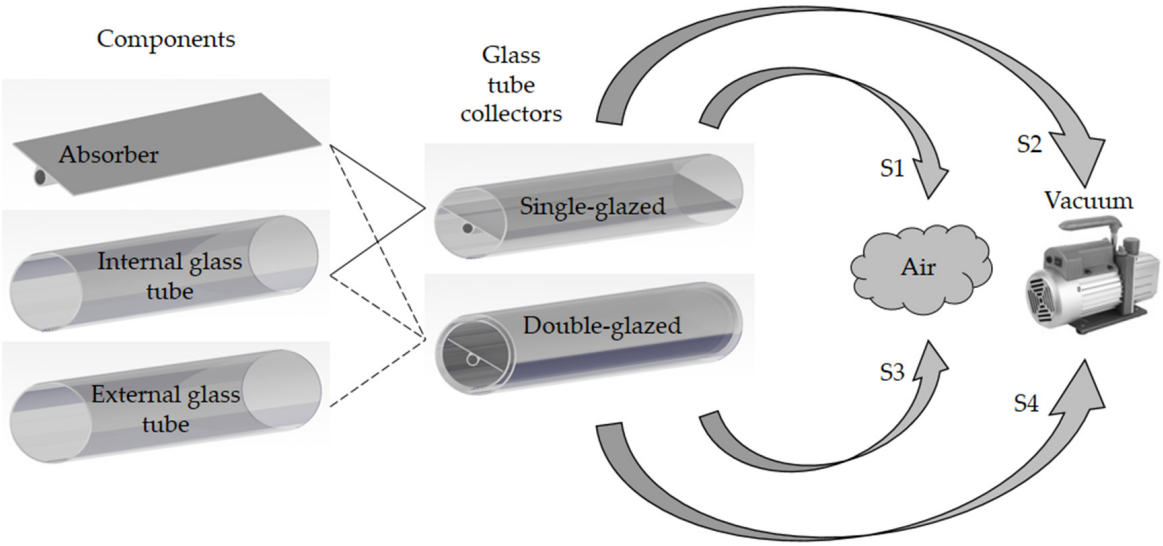

Figure 1. GTC construction types.

The basic structural and functional unit of all GTCs is the aluminum flat absorber plate (ABS) with an integrated circular cross-section flow channel (Figure 1). A selective $SnAl_2O_3$ coating is used to enhance the optical characteristics (absorptivity and emissivity [19]) of the ABS. The internal glass tube (IGT) is a common component for both SGTCs and DGTCs, while the external glass tube (EGT) is characteristic only of DGTCs. The space between the ABS and the IGT is filled with an air layer for the S1 collector type, whereas a vacuum layer is used for the S2 collector type. In the S3 collector type, two air layers are present: one between the ABS and the IGT and another between the IGT and the EGT. In the S4 collector type, these two air layers are replaced with two vacuum layers.

The geometric characteristics of the GTCs are shown in Figure 2. As illustrated, the width of the ABS is 100 mm, and its thickness is 2 mm. The diameter of the cross-section flow channel is Ø15 mm. The thickness of both the IGT and EGT is 3 mm. The distance between them (in the case of DGTCs) is 6 mm. The lengths of all components (ABS, IGT, and EGT) are 800 mm. The optical–thermal characteristics of the GTCs are presented in Table 1.

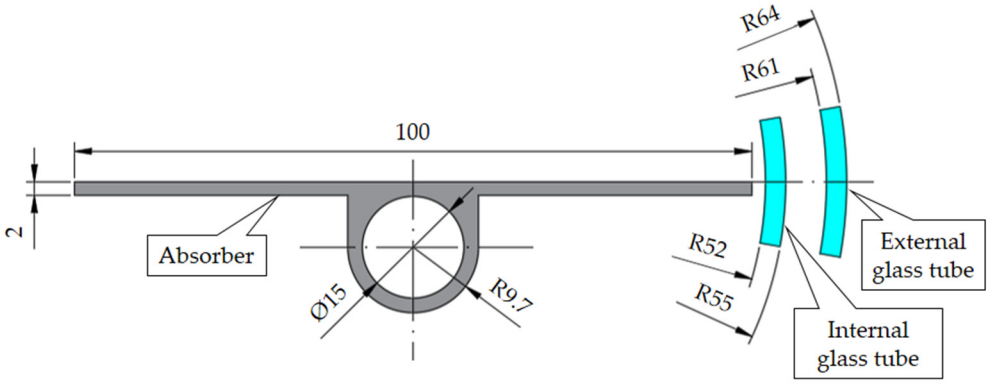

Figure 2. DGTC view in the transverse plane.

Table 1. Geometric and thermal characteristics of the GTCs [19,35,36].

Component	Material	ρ	c_p	k	ε	L
ABS	Aluminum	2700	900	203	0.25	0.8
IGT	Glass	2200	660	0.8	0.9	
EGT						

where ρ [kg/m^3] is the density, c_p [J/(kgK)] is the specific heat, k [W/(mK)] is the thermal conductivity, ε [-] is the emissivity, and L [m] is the length.

3. Materials and Methods

To effectively analyze and optimize the performance of glass tube collectors (GTCs), it is crucial to understand the mechanisms of heat loss. Heat losses (Q_{loss}) in GTCs can be described using a thermal resistance model that accounts for various components of resistance along the heat transfer path. This model enables precise calculation of the amount of heat lost by the collector, which is essential for improving its energy efficiency.

3.1. General Thermal Resistance Model for GTCs

Heat losses Q_{loss} [W] in the GTCs can be described as Equation (1) [37]:

$$Q_{loss} = \frac{T_{abs} - T_o}{\sum R_{loss}} = \frac{T_{abs} - T_o}{\sum R_{loss,\perp} + \sum R_{loss,\angle}} \approx \frac{T_{abs} - T_o}{\sum R_{loss,\perp}} \quad (1)$$

where T_{abs} [K] is the absorber temperature, T_o [K] is the ambient temperature, ΣR_{loss} [K/W] is the total resistance to heat transfer [35], $\Sigma R_{loss,\perp}$ [K/W] is the total resistance to heat transfer in the transverse plane, and $\Sigma R_{loss,\angle}$ [K/W] is the total resistance to heat transfer in the longitudinal (resistance to heat transfer in the longitudinal plane is negligibly small compared to resistance to heat transfer in the transverse plane [19]) plane.

3.1.1. Thermal Resistance Model for SGTCs

In this case (for SGTCs), the total thermal resistance to heat transfer (in the transverse plane) can be calculated as Equation (2) [38]:

$$\sum R_{loss} \approx \sum R_{loss,\perp} \approx R_{abs\text{-}igt} + R_{igt} + R_{igt\text{-}o} \quad (2)$$

where $R_{abs\text{-}igt}$ [K/W] is the resistance to heat transfer between the absorber and the internal glass tube, R_{igt} [K/W] is the resistance to heat transfer through the internal glass tube, and $R_{igt\text{-}o}$ [K/W] is the resistance to heat transfer between the internal glass tube and the ambient air.

The next figure (Figure 3) illustrates the heat transfer and resistance network for the two analyzed SGTC types: SGTC with an air layer (Figure 3a) and SGTC with a vacuum layer (Figure 3b). For the SGTC with an air layer, thermal energy (heat losses) between the

ABS and the IGT is exchanged through radiation and convection. In contrast, for the SGTC with a vacuum layer, the convective component is eliminated.

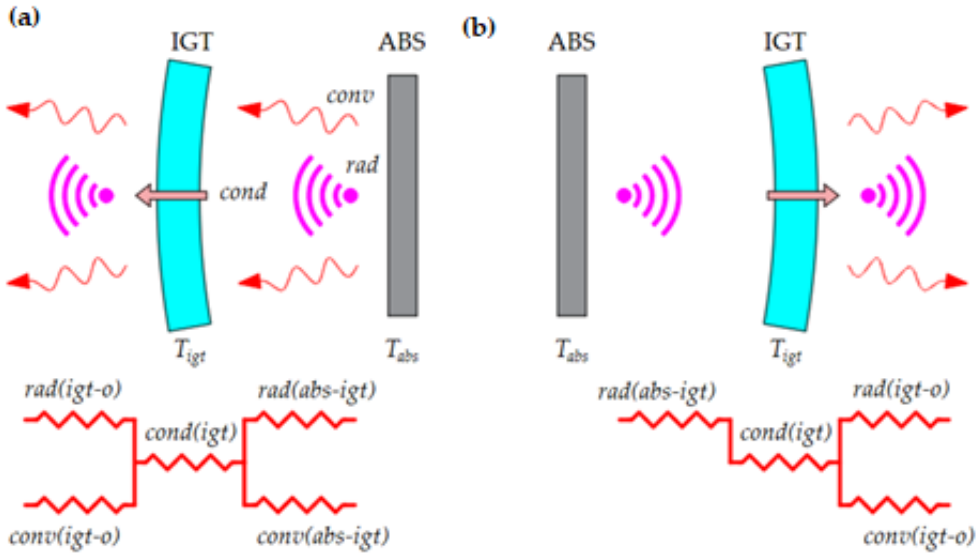

Figure 3. Heat transfer and resistance network for SGTC with an air layer (**a**) and SGTC with a vacuum layer (**b**): T_{igt} [K] is the internal glass tube temperature.

All values presented in Equation (2) are calculated using the simple and double iterative calculation algorithm (calculation method developed for this study). Figure 4 shows an iterative calculation algorithm for SGTC with an air layer.

$$h_{rad(abs\text{-}igt)} = \frac{\left(T_{abs}^2 + T_{igt}^2\right)\left(T_{abs} + T_{igt}\right)}{\frac{1}{\sigma\varepsilon_{abs}} + \frac{A_{abs,e,tot}}{A_{igt,i,tot}}\left(\frac{1}{\sigma\varepsilon_{igt}} - \frac{1}{\sigma}\right)} \tag{3}$$

$$h_{conv(abs\text{-}igt)} = \frac{Nu_{ia}k_{ia}}{D_{igt,i,eq}} \tag{4}$$

$$h_{rad(igt\text{-}o)} = \sigma\varepsilon_{igt}\left(T_{igt}^2 + T_o^2\right)\left(T_{igt} + T_o\right) \tag{5}$$

$$h_{conv(igt\text{-}o)} = 2.8 + 3W \tag{6}$$

where [39,40] σ [W/(m^{2}K^4)] is the Stefan–Boltzmann constant, $A_{igt,i,tot}$ [m^2] is the total internal area of the internal glass tube, Nu_{ia} [-] is the Nusselt number of the internal air layer [41–44], k_{ia} [W/(mK)] is the thermal conductivity of the internal air layer, $D_{igt,i,eq}$ [m] is the equivalent diameter of the internal air layer, and W [m/s] is the wind speed.

Before entering the calculation algorithm, two data groups must be adopted: SGTC geometric, thermal, and optical characteristics (Chapter 2)—first group, and meteorological parameters (values T_o and W)—second group. After that, the first stage (step I) of calculation is approached—adopting initial values of T_{abs} and T_{igt}. In step II, Equations (3)–(6) are used to determine all components in Equation (2) and then the total heat losses from Equation (1). In step III, the control $q_{abs\text{-}igt}$ and $q_{igt\text{-}o}$ equations are used to check the agreement of the adopted T_{abs} and T_{igt} values with the obtained results $q_{abs\text{-}igt} \approx q_{igt\text{-}o}$ (step IV) [45]. If the control heat flux results were approximately equal ($q_{abs\text{-}igt} \approx q_{igt\text{-}o}$, i.e., deviation ≤ 0.1 W/m^2), the iterative procedures would be completed, and the results would be finally printed (step V).

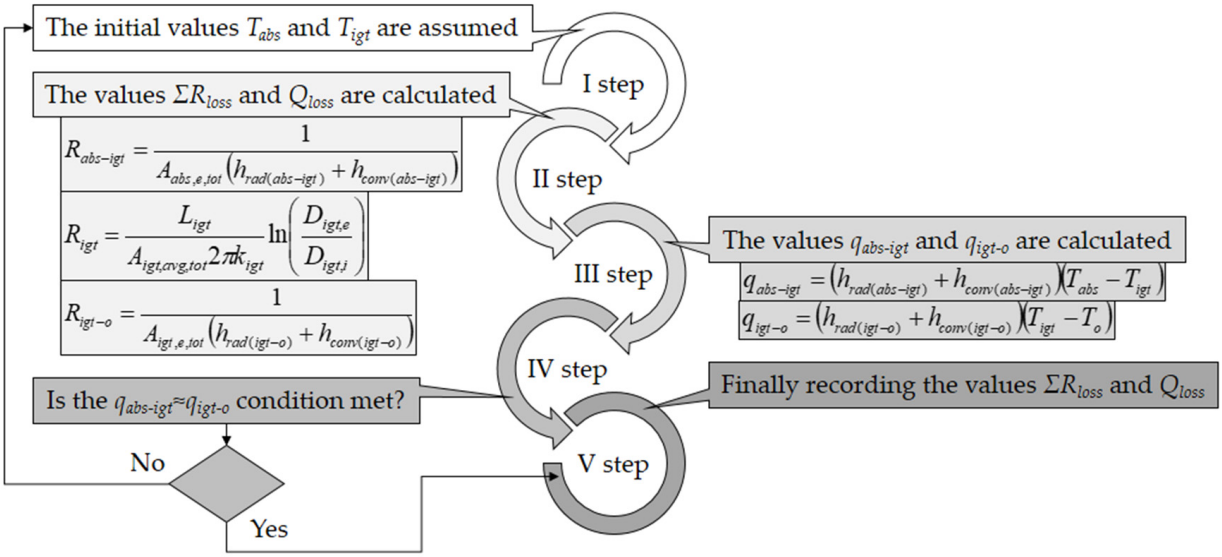

Figure 4. Double iterative calculation algorithm for SGTC with an air layer [35–37]: $A_{abs,e,tot}$ [m^2] is the total external area of the absorber, $h_{rad(abs-igt)}$ [$W/(m^2K)$] is the radiation heat transfer coefficient between the absorber and the internal glass tube (Equation (3)), $h_{conv(abs-igt)}$ [$W/(m^2K)$] is the convection heat transfer coefficient between the absorber and the internal glass tube (Equation (4)), $A_{igt,avg,tot}$ [m^2] is the total average area of the internal glass tube, $D_{igt,e}$ [m] is the external diameter of the internal glass tube, $D_{igt,i}$ [m] is the internal diameter of the internal glass tube, $A_{igt,e,tot}$ [m^2] is the total external area of the internal glass tube, $h_{rad(igt-o)}$ [$W/(m^2K)$] is the radiation heat transfer coefficient between the internal glass tube and the ambient air (Equation (5)), $h_{conv(igt-o)}$ [$W/(m^2K)$] is the convection heat transfer coefficient between the internal glass tube and the ambient air (Equation (6)), $q_{abs-igt}$ [W/m^2] is the specific heat flux exchanged between the absorber and the internal glass tube, and q_{igt-o} [W/m^2] is the specific heat flux exchanged between the internal glass tube and the ambient air.

3.1.2. Thermal Resistance Model for DGTCs

The total thermal resistance to heat transfer for DGTCs is given by Equation (7) [38]:

$$\sum R_{loss} \approx \sum R_{loss,\perp} \approx R_{abs\text{-}igt} + R_{igt} + R_{igt\text{-}egt} + R_{egt} + R_{egt\text{-}o} \quad (7)$$

where $R_{igt\text{-}egt}$ [K/W] is the resistance to heat transfer between the internal and external glass tubes, R_{egt} [K/W] is the resistance to heat transfer through the external glass tube, and $R_{egt\text{-}o}$ [K/W] is the resistance to heat transfer between the external glass tube and the ambient air.

On the one side, values $R_{abs\text{-}igt}$ and $R_{igt\text{-}egt}$ could be a function of the *rad*(*abs-igt*) and *conv*(*abs-igt*), that is, in the function of the *rad*(*igt-egt*) and *conv*(*igt-egt*)—for air layers (Figure 5a). On the other side, for vacuum layers (Figure 5b), the same values are only in function of the *rad*(*abs-igt*) and *rad*(*igt-egt*), respectively.

Due to the larger number of boundary (glass) surfaces in the construction of DGTCs, the iterative calculation algorithm should satisfy one more criterion—based on a triple check (calculation method developed for this study). For example, for triple-glazed tube collectors (TGTCs), the iterative calculation algorithm would be based on a quadruple check. In Figure 6, the triple iterative calculation algorithm for a double-glazed tube collector (DGTC) with an air layer is shown. This algorithm incorporates various parameters and coefficients, including heat transfer coefficients and areas, which are essential for accurate thermal analysis. Each coefficient and parameter depicted in the figure plays a crucial role in determining the overall thermal performance of the DGTC.

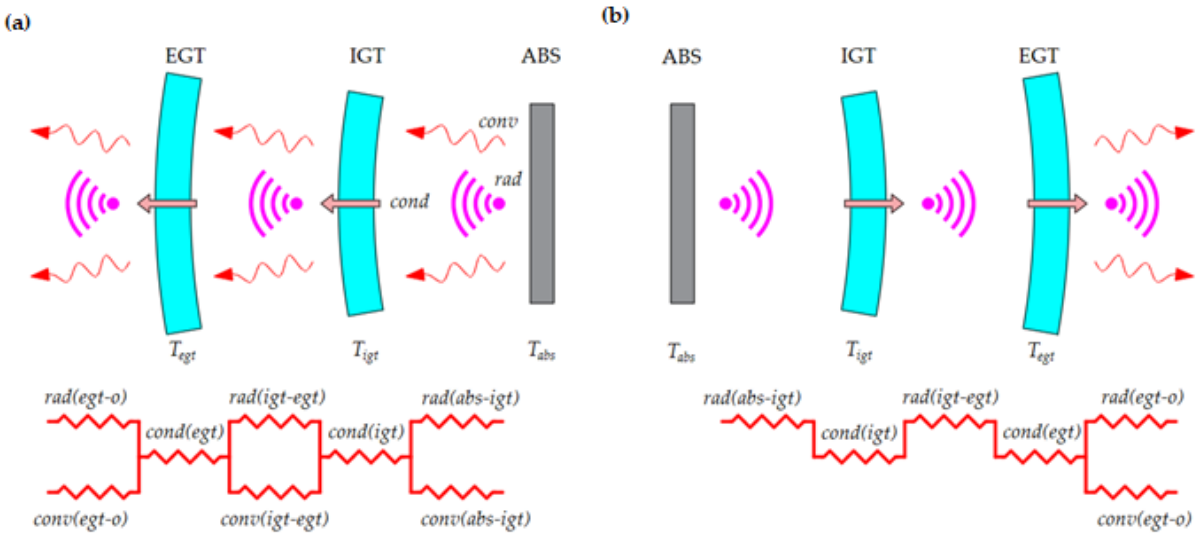

Figure 5. Heat transfer and resistance network for DGTC with an air layer (**a**) and DGTC with a vacuum layer (**b**): T_{egt} [K] is the external glass tube temperature.

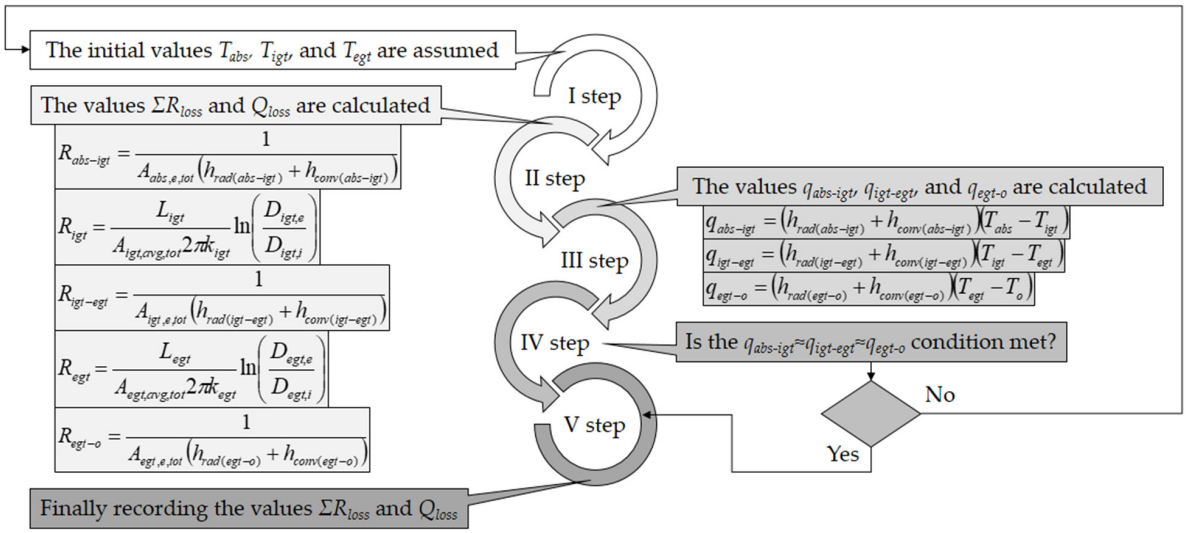

Figure 6. Triple iterative calculation algorithm for DGTC with an air layer [38–41].

The figure illustrates the calculation process involving various heat transfer coefficients and areas. Specifically, $h_{rad(igt\text{-}egt)}$ [W/(m^{2}K)] is the radiation heat transfer coefficient between the internal and the external glass tubes (Equation (8)), $h_{conv(igt\text{-}egt)}$ [W/(m^{2}K)] is the convection heat transfer coefficient between the internal and external glass tubes (Equation (9)), $A_{egt,avg,tot}$ [m^2] is the total average area of the external glass tube, $D_{egt,e}$ [m] is the external diameter of the external glass tube, $D_{egt,i}$ [m] is the internal diameter of the external glass tube, $A_{egt,e,tot}$ [m^2] is the total external area of the external glass tube, $h_{rad(egt\text{-}o)}$ [W/(m^{2}K)] is the radiation heat transfer coefficient between the external glass tube and the ambient air (Equation (10)), $h_{conv(egt\text{-}o)}$ [W/(m^{2}K)] is the convection heat transfer coefficient between the external glass tube and the ambient air (Equation (11)), $q_{igt\text{-}etg}$ [W/m^2] is the specific heat flux exchanged between the internal and external glass tubes, and $q_{etg\text{-}o}$ [W/m^2] is the specific heat flux exchanged between the external glass tube and the ambient air.

$$h_{rad(igt\text{-}egt)} = \frac{\left(T_{igt}^2 + T_{egt}^2\right)\left(T_{igt} + T_{egt}\right)}{\frac{1}{\sigma\varepsilon_{igt}} + \frac{A_{igt,e,tot}}{A_{egt,i,tot}}\left(\frac{1}{\sigma\varepsilon_{egt}} - \frac{1}{\sigma}\right)} \quad (8)$$

$$h_{conv(igt\text{-}egt)} = \frac{Nu_{ea}k_{ea}}{D_{egt,i,eq}} \quad (9)$$

$$h_{rad(egt\text{-}o)} = \sigma\varepsilon_{egt}\left(T_{egt}^2 + T_o^2\right)\left(T_{egt} + T_o\right) \quad (10)$$

$$h_{conv(egt\text{-}o)} = 2.8 + 3W \quad (11)$$

where [39,40] Nu_{ea} [-] is the Nusselt number of the external air layer [41–44], k_{ea} [W/(mK)] is the thermal conductivity of the external air layer, and $D_{igt,i,eq}$ [m] is the equivalent diameter of the external air layer.

In step I of the triple iterative calculation algorithm (Figure 6), the initial values are T_{abs}, T_{igt}, and T_{egt}. All Equation (7) values are determined in step II using Equations (3), (4), and (8)–(11). The control equations (step III) now are $q_{abs\text{-}igt}$, $q_{igt\text{-}egt}$, and $q_{egt\text{-}o}$ [45]. When the control heat flux results were approximately equal ($q_{abs\text{-}igt} \approx q_{igt\text{-}egt} \approx q_{egt\text{-}o}$, with the same deviation, step IV), the calculation would be finished (step V).

3.2. Experimental Model

Experimental validation of the analytical (mathematical) model was performed on the example of the SGTC with an air layer (S1 collector type, Chapter 2). The isometric view of the mentioned SC is shown in Figure 7a, while the complete experimental installation with the measuring chain is shown in Figure 7b.

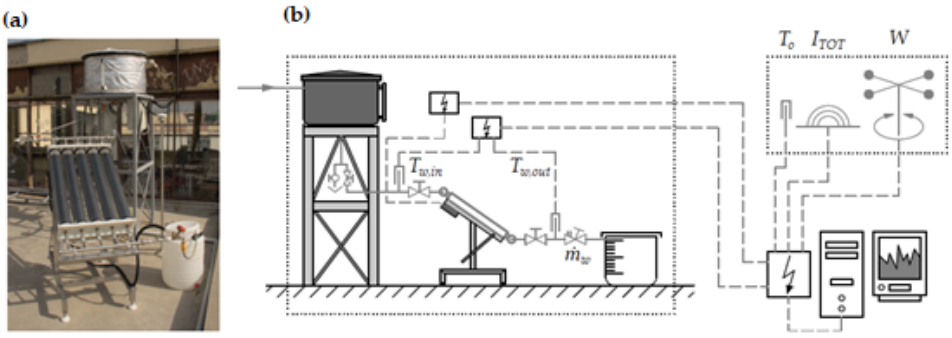

Figure 7. View of the SGTC with an air layer (**a**) and experimental installation with a measuring chain (**b**) [46].

The experimental installation with a measuring chain (Figure 7b) is formed by two subsystems: solar construction (Figure 7a) and a meteorological station. The experimental installation operation principle with open circulation circuits (without circulation pumps) is based on hydrostatic pressure—the driving force for water flow through the SC. Accompanying measuring equipment for collecting appropriate parameters (solar irradiance intensity on a horizontal surface, ambient air temperature, wind speed, water inlet temperature, water outlet temperature, and water mass flow rate) required for thermal analysis consisted of a Kipp & Zonen SMP3 pyranometer (accuracy < 5%), a Kipp & Zonen data logger METEON (accuracy < 0.1%), WZP-035 Ø5 × 50 mm Pt-100 temperature probes (accuracy ± 0.2 °C), and a HERZ STROMAX manual control valve [19].

Experimental Q_{loss} value was measured indirectly by Equation (12):

$$Q_{loss} = Q_{sun} - Q_{heat} = A_{abs(up)}I_{TOT} - \dot{m}_w c_p(T_{w,out} - T_{w,in}) \quad (12)$$

where Q_{sun} [W] is the solar heat power, Q_{heat} [W] is the heat power of the SGTC with an air layer, $A_{abs(up)}$ [m^2] is the upside area of the absorber, I_{TOT} [W/m^2] is the total incident solar irradiance (for the tilted surfaces, the value I_{TOT} is mathematically calculated according to the recommendations from [43]), $\dot{m}_w$ [kg/s] is the mass flow rate of the water, $T_{w,out}$ [K] is the outlet temperature of the water, and $T_{w,in}$ [K] is the inlet temperature of the water.

3.3. Multi-Criteria Decision-Making Method

The optimal solar design (dimensioning and selection) of the presented GTCs (Figure 1) is determined using three groups of indicators: geometric (mass m [kg], surface occupation SO [m^2], total surface occupation TSO [m^2], volume occupation VO [m^3]), economic (manufacturing cost CM [EUR] and exploitation cost CE [EUR]), and ecological (embodied energy E_{emb} [kWh] and greenhouse gas emissions e_{CO2} [kg]).

A multidisciplinary evaluation of GTC performance can be conducted using various multi-criteria analysis (MCA) methods [47]. Due to its simplicity and accuracy, the multi-criteria decision-making (MCDM) method with simple additive weighting (SAW) was chosen for this paper [48,49].

The MCDM method assigns a specific percentage criterion of importance, i.e., weight of significance (w_c [%] and w_{sc} [%]), to all indicators used (Table 2).

Table 2. The weight of importance to all used indicators.

Criterion	Geometric				Economic		Ecological		C-sum
w_c	14				50		36		100
Sub-criterion	***m***	***SO***	***TSO***	***VO***	***CM***	***CE***	E_{emb}	e_{CO2}	**SC-sum**
w_{sc}	5	5	2	2	35	15	18	18	100

By defining w_c and w_{sc} values, all included indicators (in this case, eight of them, as shown in Table 2) are normalized to a dimensionless level. Only then can their classification in descending or ascending order, depending on the desired objective (the objective function), be performed. In this case, the objective function is minimizing heat losses in GTCs. The following figure (Figure 8) illustrates the procedure for selecting the mentioned objective function.

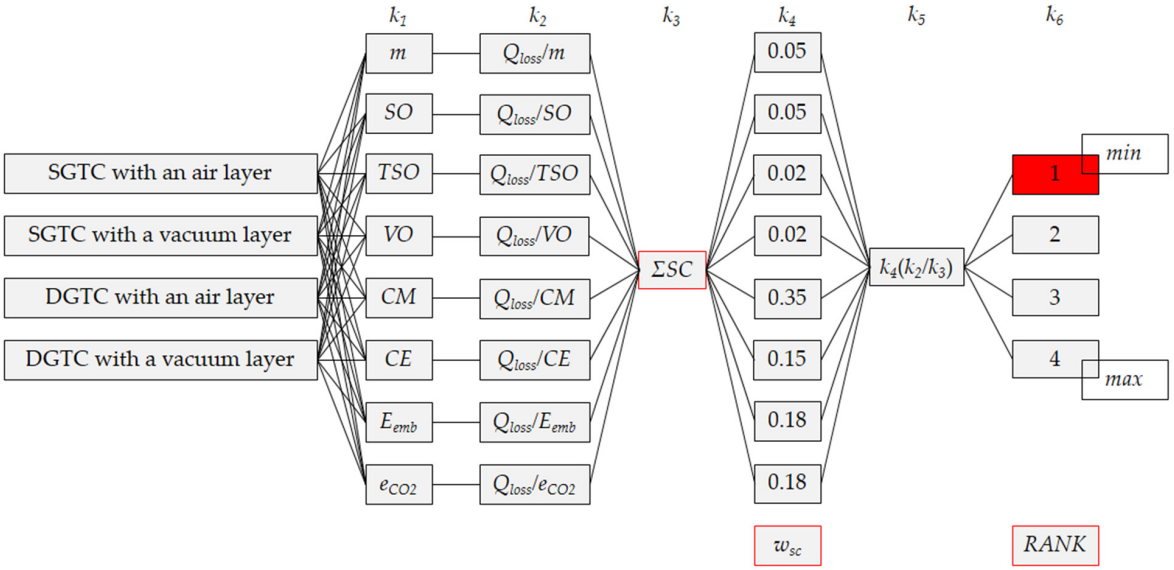

Figure 8. Multi-criteria decision-making method with simple additive weighting in the function of selecting GTC type.

In the first two steps, numerous values of all sub-criteria, i.e., indicators (k_1 values: m, SO, TSO, VO, CM, CE, E_{emb}, and e_{CO2}) and specific indicators (k_2 values: Q_{loss}/m, Q_{loss}/SO, Q_{loss}/TSO, Q_{loss}/VO, Q_{loss}/CM, Q_{loss}/CE, Q_{loss}/E_{emb}, and Q_{loss}/e_{CO2}), are defined for all GTC types. In the third step, k_3 values are calculated as in Equation (13), while in the fifth step, values k_5 are a function of k_2, k_3, and k_4, as shown Figure 8.

$$k_3 = \left(\frac{Q_{loss}}{m}\right)_{SGTCa} + \left(\frac{Q_{loss}}{m}\right)_{SGTCv} + \left(\frac{Q_{loss}}{m}\right)_{DGTCa} + \left(\frac{Q_{loss}}{m}\right)_{DGTCv} \quad (13)$$

Equation (13) represents the sum of Q_{loss}/m specific indicators for an SGTC with an air layer, SGTC with a vacuum layer, DGTC with an air layer, and DGTC with a vacuum layer. Based on this equation, the remaining seven equations can also be developed (for the other specific indicators).

Determining the k_5 values in the fifth step is shown in the example of the SGTC with an air layer taking into account specific indicator Q_{loss}/m (Equation (14)):

$$k_5 = k_4 \frac{k_2}{k_3} = 0.05 \frac{\left(\frac{Q_{loss}}{m}\right)_{SGTCa}}{\left(\frac{Q_{loss}}{m}\right)_{SGTCa} + \left(\frac{Q_{loss}}{m}\right)_{SGTCv} + \left(\frac{Q_{loss}}{m}\right)_{DGTCa} + \left(\frac{Q_{loss}}{m}\right)_{DGTCv}} \quad (14)$$

In the final stage, the values obtained from the fifth step are classified (sixth step, k_6 values) to identify the minimum value, which represents the objective function. This process concludes the calculation.

The subsequent table (Table 3) presents the adopted geometric indicators (as per the data in Table 1), along with the economic and ecological indicators. The ecological indicators include embodied energy (Equation (15)) and greenhouse gas emissions (Equation (16)) [50] for the analyzed GTC constructions.

$$E_{emb} = \frac{mE_{emb,spec}}{20} \quad (15)$$

$$e_{CO2} = e_{CO2,spec}E_{pry} = e_{CO2,spec}K_{pry}E_{fin} = e_{CO2,spec}K_{pry}\frac{E_{loss}time}{1000\eta_{el}} \quad (16)$$

where [47] $E_{emb,spec}$ [kWh/kg] is the specific embodied energy ($E_{emb,spec}$ = 53 kWh/kg for aluminum [51], and $E_{emb,spec}$ = 25.8 kWh/kg for glass [52]), $e_{CO2,spec}$ [kg/kWh] is the specific CO_2 emission (For electricity [50], $e_{CO2,spec}$ = 0.53 kg/kWh, while K_{pry} = 2.5), E_{pry} [kWh] is the primary energy consumption, K_{pry} [-] is the primary energy transformation coefficient[11], E_{fin} [kWh] is the final energy consumption, *time* [h] is the working time[8], η_{el} [-] is the efficiency of the electric boiler (η_{el} = 0.98 for electric boiler).

Table 3. Geometric, economic, and ecological indicators for analyzed GTC constructions [50–52].

Main Components									
Element	***V***	***m***	***SO***	***TSO***	***VO***	***CM***	***CE***	E_{emb}	e_{CO2}
ABS	0.000253	0.683	0.08	0.184	0.00049	25	13	1.81	-
IGT	0.000807	1.775	0.088	0.276	0.0076	76	38	2.29	-
EGT	0.000943	2.075	0.1024	0.322	0.0103	91	46	2.68	-
Glass tube collector types									
Model		***m***	***SO***	***TSO***	***VO***	***CM*** [1]	***CE*** [2]	E_{emb}	e_{CO2} [3]
SGTC with an air layer		2.458	0.088	0.276	0.0076	101	51	4.1	1303
SGTC with a vacuum layer						111	56		809
DGTC with an air layer		4.533	0.1024	0.322	0.0103	192	96	6.78	2215
DGTC with a vacuum layer						221	111		1418

[1] The *CM* [EUR] for SGTC with a vacuum layer increase by 10% compared to SGTC with an air layer. The same costs for DGTC with a vacuum layer increase by 15% compared to DGTC with an air layer. [2] In all cases, the exploitation costs *CE* [EUR] during the 20 years (adopted working time) are 50% of the CM. The same time period is taken for the calculation of ecological indicators E_{emb} and e_{CO2}. [3] CO_2 emission cannot be determined without knowing the E_{loss} value (Equation (16), Chapter 4).

Equation (16) is used when thermal energy needs to be provided from another energy source. In this case, it is an electric boiler because it is one of Serbia's most common heat-energy generators [50].

4. Results and Discussion

Figure 9 shows Q_{loss} and t_{igt} in the SGTC with an air layer (Figure 9a) and SGTC with a vacuum layer (Figure 9b) for previously adopted t_{abs}, t_o and W values.

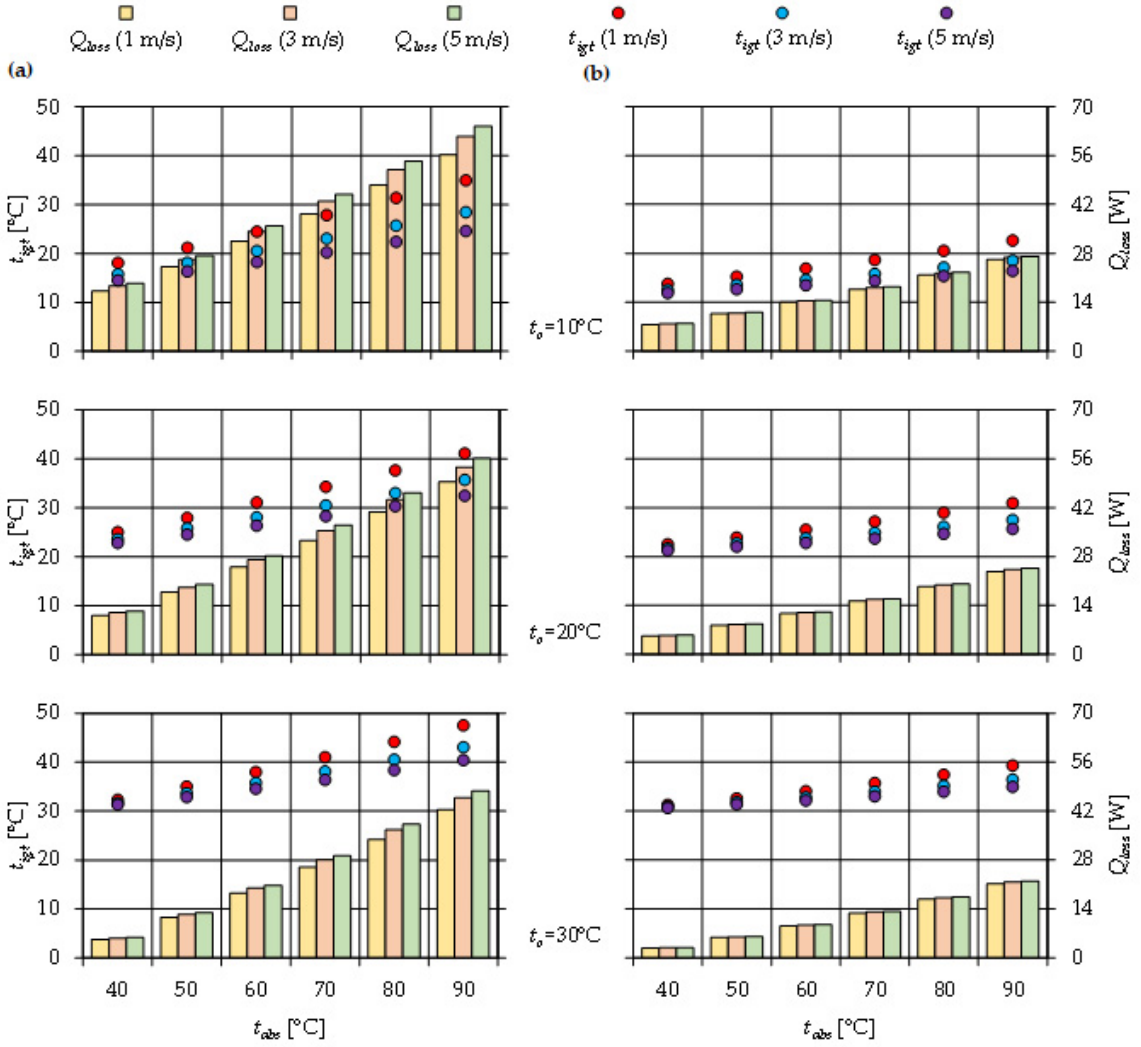

Figure 9. Characteristic temperatures and heat losses for SGTC with an air layer (**a**) and SGTC with a vacuum layer (**b**).

All diagrams (Figure 9) were formed by varying the following three values: t_{abs} (40 °C, 50 °C, 60 °C, 70 °C, 80 °C and 90 °C)—first variable, t_o (10 °C, 20 °C, and 30 °C)—second variable, and W (1 m/s, 3 m/s, and 5 m/s)—third variable.

Figure 9 shows that the heat losses in the SGTCs (SGTC with an air and SGTC with a vacuum layer) increase with the increase in the temperature of the absorber and the increase in the wind speed. A higher absorber temperature increases the temperature difference with the environment, so the driving force of the heat losses increases. When the wind is faster, convective component Equation (6) is higher, and heat losses increase. Wind speed also determines the temperature of the glass (these values are proportional). Contrary to that, higher ambient temperature causes the opposite effect. When the ambient temperature increases, the temperature difference between the environments decreases [53,54].

When t_o = 10 °C and W = 1 m/s (Figure 9a), heat losses in the SGTC with an air layer are between 17.17 W (for t_{abs} = 40 °C) and 56.27 W (for t_{abs} = 90 °C). The heat losses are higher 8.54–9.25% (W = 3 m/s) and 13.17–14.49% (W = 5 m/s) for the same ambient temperature. If the second variable is t_o = 20 °C, the heat losses are within the following limits: 11.14–49.37 W (W = 1 m/s), 12–53.65 W (W = 3 m/s), and 12.47–56.11 W

(W = 5 m/s). Maximum (for t_{abs} = 90 °C) heat loss values are the lowest when t_o = 30 °C: 42.37 W (W = 1 m/s), 45.82 W (W = 3 m/s), and 47.81 W (W = 5 m/s). The highest and lowest internal glass tube temperatures for the SGTC with an air layer are (Figure 9a): t_{igt} = 47.5 °C (for t_o = 30 °C, t_{abs} = 90 °C, and W = 1 m/s), and t_{igt} = 14.49 °C (for t_o = 10 °C, t_{abs} = 40 °C, and W = 5 m/s).

The calculation algorithm (Figure 4) for the SGTC with a vacuum layer is simpler due to the elimination of the convective component of Equation (4). The same effect explains the reduction of the heat losses (Figure 9b). For example, from 64.42 W to 27.11 W (t_o = 10 °C, t_{abs} = 90 °C, and W = 5 m/s) is the best case scenario. In this case, the value t_{igt} is in the following range: t_{igt} = 11.87 °C (for t_o = 10 °C, t_{abs} = 40 °C, and W = 5 m/s) and t_{igt} = 39.3 °C (for t_o = 30 °C, t_{abs} = 90 °C, and W = 1 m/s).

Analogous to the previous figure (Figure 9), the next figure (Figure 10) shows Q_{loss} and t_{igt} in the DGTC with an air layer (Figure 10a) and DGTC with a vacuum layer (Figure 10b) for previously adopted t_{abs}, t_o and W values.

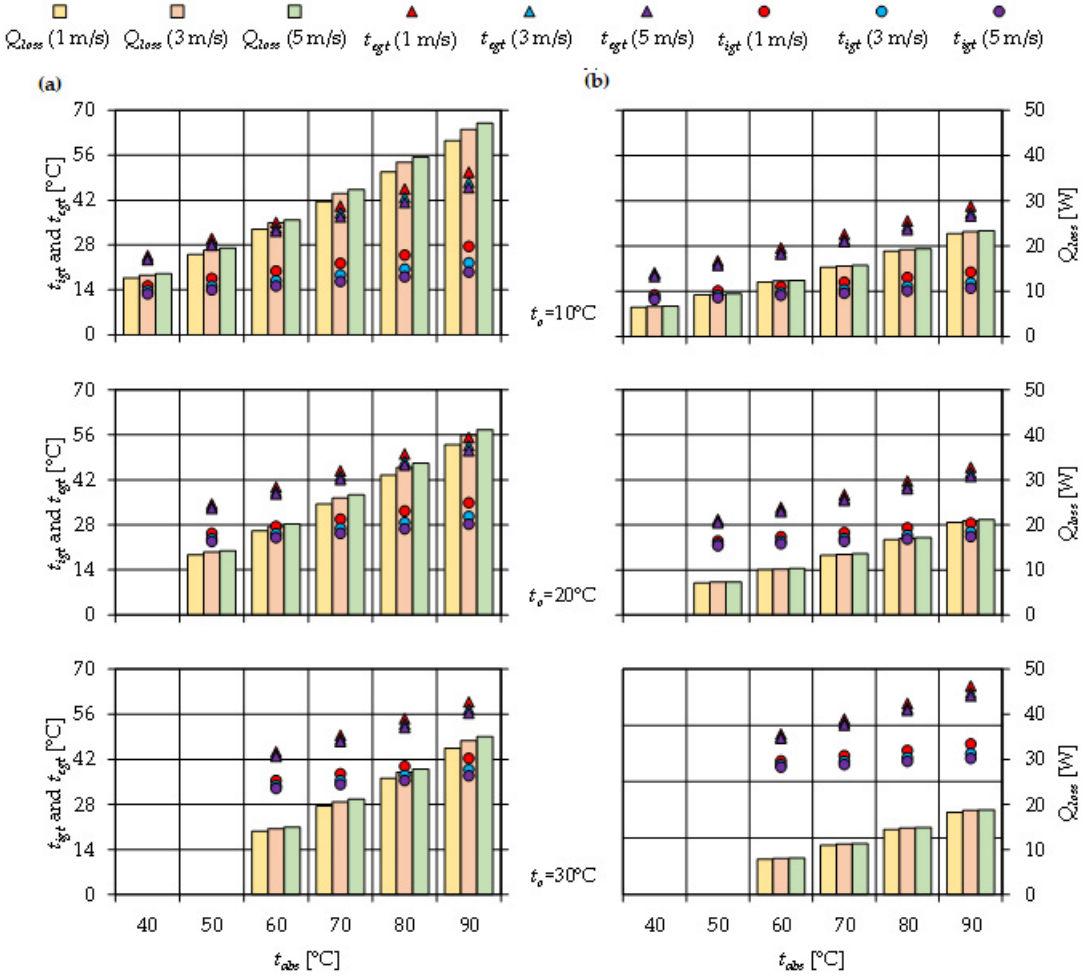

Figure 10. Characteristic temperatures and heat losses for DGTC with an air layer (**a**) and DGTC with a vacuum layer (**b**).

When it comes to the DGTCs (DGTC with an air layer and DGTC with a vacuum layer), the conclusions are the same as in the case of the SGTCs (Figure 10): heat losses are proportional to the absorber temperature, heat losses are proportional to the wind speed, and heat losses are inversely proportional to the ambient temperature.

For the DGTC with an air layer (Figure 10a), heat losses are the highest (Q_{loss} = 47.14 W) when t_o = 10 °C, t_{abs} = 90 °C, and W = 5 m/s and the smallest (Q_{loss} = 12.65 W) when t_o = 10 °C, t_{abs} = 40 °C, and W = 1 m/s. The internal glass tube temperatures are between

t_{igt} = 23.4 °C (t_o = 10 °C, t_{abs} = 40 °C, and W = 5 m/s) and t_{igt} = 59.8 °C (t_o = 30 °C, t_{abs} = 90 °C, and W = 1 m/s). In contrast, the external glass tube temperatures are between t_{egt} = 12.8 °C and t_{egt} = 42.3 °C (the same boundary conditions apply as for t_{igt}).

The highest Q_{loss} = 23.35 W (t_o = 10 °C, t_{abs} = 90 °C, and W = 5 m/s) and the smallest Q_{loss} = 6.48 W (t_o = 10 °C, t_{abs} = 40 °C, and W = 1 m/s) heat losses in the DGTC with a vacuum layer can be seen in Figure 10b. Compared with the DGTC with an air layer, heat losses in the DGTC with a vacuum layer are on average 1.92 times lower (maximum is 2.07 times, minimum is 1.78 times). The internal glass tube temperatures are between t_{igt} = 18.6 °C and t_{igt} = 51.8 °C. The external glass tube temperatures are between t_{egt} = 11.4 °C and t_{egt} = 37.4 °C.

The diagrams in Figure 10 are interesting because of another phenomenon. Namely, it can be seen that the analytical calculation results are missing when t_o = 20 °C (t_{abs} = 40 °C). They are also missing when t_o = 30 °C (t_{abs} = 40 °C and t_{abs} = 50 °C). This anomaly is characteristic of the triple iterative calculation algorithm for DGTCs (Figure 6). As the ambient temperature increases, the convergence of results for values of tabs close to that is impossible. Temperatures t_{abs}, t_{igt}, and t_{egt} are approaching, while the control equations tend to divagation. It proves that DGTCs operate at higher operating temperatures than SGTCs.

Experimental validation of the heat losses analytical model for the SGTC with an air layer is shown in Figure 11 (for t_o = 20 °C) and Figure 12 (for t_o = 30 °C).

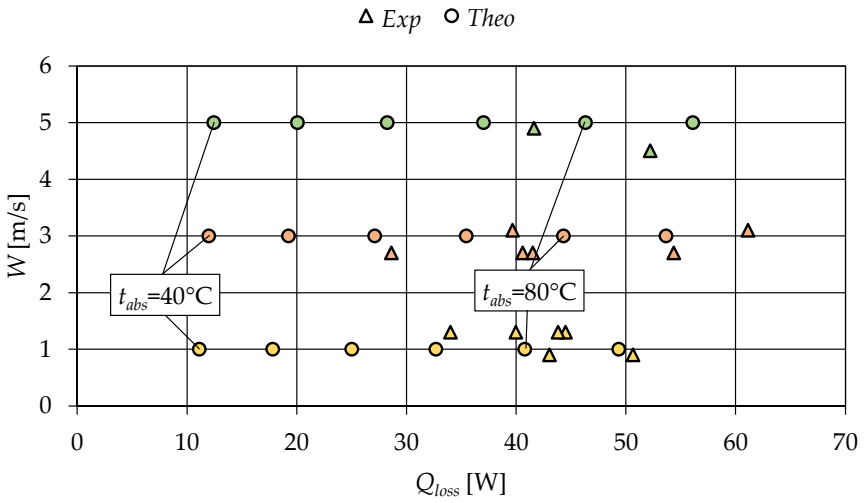

Figure 11. Experimental validation results of SGTC with an air layer for t_o = 20 °C.

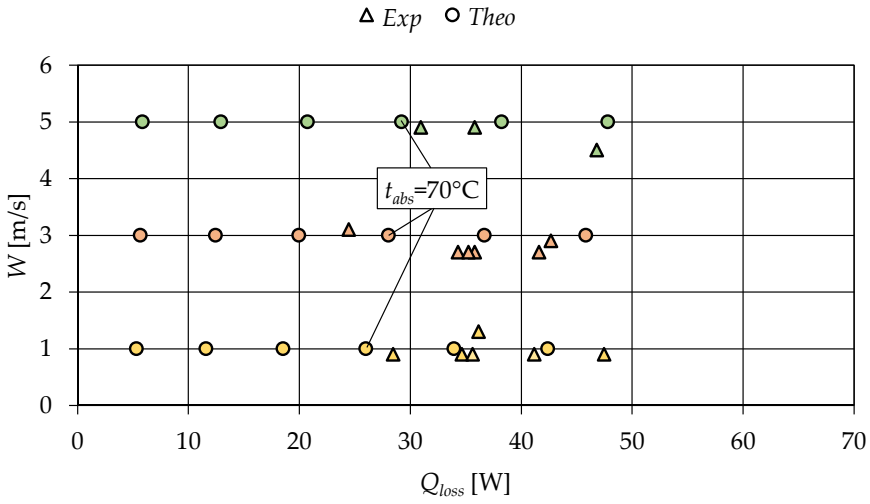

Figure 12. Experimental validation results of SGTC with an air layer for t_o = 30 °C.

Experimental heat losses were determined using Equation (12), as previously described. The Q_{loss} values were obtained from a four-month measurement period (15 July to 15 October 2021), ensuring that the experimental values for t_o and W align with the corresponding values used in the mathematical (analytical) model. This alignment provided the necessary conditions to validate the model for initial research on glass tube collectors (GTCs). The validated model is designed to function without requiring additional inputs, such as solar radiation intensity or mass flow rate, while maintaining accuracy within the desired limits.

As illustrated in Figure 11, the experimental data points grouped between t_{abs} = 70 °C and t_{abs} = 90 °C (W = 1 m/s and W = 3 m/s) and between t_{abs} = 60 °C and t_{abs} = 90 °C (W = 2 m/s). Similar phenomena are shown in Figure 12. If it is known that the absorber temperature in classic single-glazed solar collectors is between 30 and 80 °C [55], it can be concluded that the presented method has accuracy within satisfactory limits. For more detailed results, it is necessary to develop mathematical models with all the specificities that characterize the solar construction.

After the theoretical analysis of the thermal performance of GTCs and experimental validations, the results of the MCDM method will be presented in detail below to determine the optimal design of GTCs.

Following Figure 9 and Table 3, Table 4 defines specific geometric, economic, and ecological indicators for optimal GTC type selection (k_2 values). In this phase (for t_o = 20 °C and W = 3 m/s), the values of heat losses (Q_{loss} with e_{CO2}, Equation (16), Table 3) were used when t_{abs} = 50 °C (SGTC with an air layer), t_{abs} = 60 °C (SGTC with a vacuum layer), t_{abs} = 80 °C (DGTC with an air layer), and t_{abs} = 90 °C (DGTC with a vacuum layer)—typical average values (Figure 9, Figure 10). In the same table (Table 4), the last column provides an insight into the values k_3 (Equation (13)).

Table 4. Specific geometric, economic, and ecological indicators.

Specific Indicator	SGTC		DGTC		Sum
	Air Layer	Vacuum Layer	Air Layer	Vacuum Layer	
$\frac{Q_{loss}}{m}$	7.84	4.87	7.23	4.63	24.56
$\frac{Q_{loss}}{SO}$	218.98	136.02	319.92	204.88	879.8
$\frac{Q_{loss}}{TSO}$	69.82	43.37	101.74	65.16	280.08
$\frac{Q_{loss}}{VO}$	2535.53	1575	3180.58	2036.89	9328
$\frac{Q_{loss}}{CM}$	0.19	0.11	0.17	0.09	0.56
$\frac{Q_{loss}}{CE}$	0.38	0.21	0.34	0.19	1.12
$\frac{Q_{loss}}{E_{emb}}$	4.7	2.92	4.83	4.48	16.93
$\frac{Q_{loss}}{e_{CO2}}$	0.01	0.01	0.01	0.01	0.06

Values of k_4 can be seen in Table 2. Values of k_5 (Equation (14)) and k_6 (ranking of indicators) from Figure 8 are shown in Table 5. The specific indicators with the lowest values are a goal function because the aim is to minimize heat losses in GTCs.

The final ranking of glass tube collectors (GTCs), derived using the multi-criteria decision-making (MCDM) method, is detailed in Table 6. The analysis reveals that simpler designs, such as the single-glazed tube collector (SGTC) with a vacuum layer, frequently emerge as superior options based on the primary geometric, economic, and ecological criteria (refer to Table 6). The double-glazed tube collector (DGTC) with a vacuum layer ranks second in the evaluation. Conversely, the single-glazed tube collector (SGTC) with an air layer occupies the lowest position according to the MCDM method results.

Table 5. Ranking of the specific geometric, economic, and ecological indicators.

Specific Indicator	SGTC		DGTC		Rank SGTC with a Vacuum Layer
	Air Layer	Vacuum Layer	Air Layer	Vacuum Layer	
$\frac{Q_{loss}}{m}$	0.0160	0.0099	0.0147	0.0094	2
$\frac{Q_{loss}}{SO}$	0.0124	0.0077	0.0182	0.0116	1
$\frac{Q_{loss}}{TSO}$	0.0050	0.0031	0.0073	0.0047	1
$\frac{Q_{loss}}{VO}$	0.0054	0.0034	0.0068	0.0044	1
$\frac{Q_{loss}}{CM}$	0.1184	0.0669	0.1058	0.0589	2
$\frac{Q_{loss}}{CE}$	0.0505	0.0286	0.0456	0.0253	2
$\frac{Q_{loss}}{E_{emb}}$	0.0500	0.0310	0.0514	0.0477	1
$\frac{Q_{loss}}{e_{CO2}}$	0.0450	0.0450	0.0450	0.0450	1

Table 6. Final ranking of GTCs.

Specific Indicator	SGTC		DGTC	
	Air Layer	Vacuum Layer	Air Layer	Vacuum Layer
Final results	0.30266	0.19563	0.29481	0.20690
Final ranking	4	1	3	2

Vacuum technology leads to increased embodied energy investments and, consequently, higher production costs. This chain reaction also results in higher maintenance costs. However, it significantly reduces heat losses by 37.88% compared to single-glazed tube collectors (SGTCs) with an air layer and by 35.96% compared to double-glazed tube collectors (DGTCs) with an air layer.

Heat losses in solar collectors represent the portion of energy that is not utilized and is instead dissipated into the environment. Although more advanced solar collector designs often exhibit higher thermal (useful) power, this does not necessarily imply a reduction in heat losses or an increase in thermal efficiency. In many cases, as the thermal power of solar collectors increases, so do the heat losses, indicating a greater amount of unused energy. Consequently, such technical challenges must be addressed with careful, multidisciplinary approaches.

5. Conclusions

In the first part of this paper, the heat losses of four types of glass tube collectors (GTCs) are analyzed mathematically: the single-glazed glass tube collector with an air layer, the single-glazed glass tube collector with a vacuum layer, the double-glazed glass tube collector with an air layer, and the double-glazed glass tube collector with a vacuum layer. Appropriate mathematical models and calculation algorithms were developed, employing double iteration for single-glazed collectors and triple iteration for double-glazed collectors. The results indicate that the minimum and maximum heat loss values Q_{loss} are as follows: 5.29 W and 64.42 W for the single-glazed collector with an air layer, 2.74 W and 27.11 W for the single-glazed collector with a vacuum layer, 12.65 W and 47.14 W for the double-glazed collector with an air layer, and 6.48 W and 23.35 W for the double-glazed collector with a vacuum layer, depending on the ambient temperature (t_o) and wind speed (W). It was concluded that heat losses are proportional to the absorber temperature and wind speed while inversely proportional to the ambient temperature.

In the second part of the paper, the theoretical results of heat losses are compared with experimental measurements obtained over a four-month period. The experimental values, which align with the theoretical values, were assessed according to two criteria: ambient

temperature and wind speed. The agreement between the theoretical and experimental models indicates that the developed calculation algorithms are validated experimentally.

In the third part of the paper, three primary groups of indicators, along with their corresponding sub-indicators, are defined to determine the optimal design of GTCs using the multi-criteria decision-making (MCDM) method with simple additive weighting (SAW). These groups include geometric indicators (mass, surface occupation, total surface occupation, volume occupation), economic indicators (production costs and exploitation costs), and ecological indicators (embodied energy and greenhouse gas emissions). The multidisciplinary analysis reveals that the single-glazed collector with a vacuum layer is the most favorable option, while the single-glazed collector with an air layer is the least favorable.

For example, the literature often neglects the inclusion of economic and ecological factors in assessing the thermal performance of solar collectors, which challenges the justification of many solar applications.

The primary objective of the proposed methodology is to offer a novel perspective for future research on the shortcomings of solar collectors and to underscore the significance of a comprehensive approach. The paper aims to provide future research with a new viewpoint on these issues by applying a simple and efficient multidisciplinary method.

Author Contributions: Conceptualization, A.N. and R.K.; Software, A.N. and D.C.; Validation, A.N., D.C. and A.J.; Formal analysis, A.N. and R.K; Investigation, A.N., R.K. and A.J.; Resources, A.N. and D.C.; Writing—original draft, A.N.; Writing—review and editing, A.N. and R.K.; Project administration, A.N. and R.K.; Funding acquisition, A.J. All authors have read and agreed to the published version of the manuscript.

Funding: This research received no external funding.

Institutional Review Board Statement: Not applicable.

Informed Consent Statement: Not applicable.

Data Availability Statement: The original contributions presented in the study are included in the article; further inquiries can be directed to the corresponding author.

Conflicts of Interest: The authors declare no conflicts of interest.

References

1. Ajeena, A.M.; Víg, P.; Farkas, I. A comprehensive analysis of nanofluids and their practical applications for flat plate solar collectors: Fundamentals, thermophysical properties, stability, and difficulties. *Energy Rep.* **2022**, *8*, 4461–4490. [CrossRef]
2. Sabiha, M.A.; Saidur, R.; Mekhilef, S.; Mahian, O. Progress and latest developments of evacuated tube solar collectors. *Renew. Sustain. Energy Rev.* **2015**, *51*, 1038–1054. [CrossRef]
3. Martínez-Rodríguez, G.; Fuentes-Silva, A.L.; Picón-Núñez, M. Solar thermal networks operating with evacuated-tube collectors. *Energy* **2018**, *146*, 26–33. [CrossRef]
4. Mazarrón, F.R.; Porras-Prieto, C.J.; García, J.L.; Benavente, R.M. Feasibility of active solar water heating systems with evacuated tube collector at different operational water temperatures. *Energy Convers. Manag.* **2016**, *113*, 16–26. [CrossRef]
5. Aramesh, M.; Shabani, B. Performance evaluation of an enhanced self-storing evacuated tube solar collector in residential water heating application. *J. Energy Storage* **2023**, *71*, 108118. [CrossRef]
6. Walker, A.; Mahjouri, F.; Stiteler, R. Evacuated-tube heat-pipe solar collectors applied to the recirculation loop in a federal building (No. NREL/CP-710-36149). In Proceedings of the American Solar Energy Society Conference, Portland, OR, USA, 11–14 July 2004.
7. García, J.L.; Porras-Prieto, C.J.; Benavente, R.M.; Gómez-Villarino, M.T.; Mazarrón, F.R. Profitability of a solar water heating system with evacuated tube collector in the meat industry. *Renew. Energy* **2019**, *131*, 966–976. [CrossRef]
8. Hassanien, R.H.E.; Li, M.; Tang, Y. The evacuated tube solar collector assisted heat pump for heating greenhouses. *Energy Build.* **2018**, *169*, 305–318. [CrossRef]
9. Bellos, E.; Papavasileiou, L.; Kekatou, M.; Karagiorgas, M. A comparative energy and economic analysis of different solar thermal domestic hot water systems for the Greek climate zones: A multi-objective evaluation approach. *Appl. Sci.* **2022**, *12*, 4566. [CrossRef]
10. Shoeibi, S.; Kargarsharifabad, H.; Rahbar, N.; Khosravi, G.; Sharifpur, M. An integrated solar desalination with evacuated tube heat pipe solar collector and new wind ventilator external condenser. *Sustain. Energy Technol. Assess.* **2022**, *50*, 101857. [CrossRef]

11. Mehta, J.R.; Rane, M.V. Liquid desiccant based solar air conditioning system with novel evacuated tube collector as regenerator. *Procedia Eng.* **2013**, *51*, 688–693. [CrossRef]
12. Al-Falahi, A.; Alobaid, F.; Epple, B. A new design of an integrated solar absorption cooling system driven by an evacuated tube collector: A case study for Baghdad, Iraq. *Appl. Sci.* **2020**, *10*, 3622. [CrossRef]
13. Chen, F.; Xia, E.T.; Bie, Y. Comparative investigation on photo-thermal performance of both compound parabolic concentrator and ordinary all-glass evacuated tube absorbers: An incorporated experimental and theoretical study. *Sol. Energy* **2019**, *184*, 539–552. [CrossRef]
14. Abo-Elfadl, S.; Hassan, H.; El-Dosoky, M.F. Energy and exergy assessment of integrating reflectors on thermal energy storage of evacuated tube solar collector-heat pipe system. *Sol. Energy* **2020**, *209*, 470–484. [CrossRef]
15. Mao, C.; Li, M.; Li, N.; Shan, M.; Yang, X. Mathematical model development and optimal design of the horizontal all-glass evacuated tube solar collectors integrated with bottom mirror reflectors for solar energy harvesting. *Appl. Energy* **2019**, *238*, 54–68. [CrossRef]
16. Chen, X.; Yang, X.; Li, M. Combining horizontal evacuated tubes with booster mirror reflector to achieve seasonal reverse output: Technical and experimental investigation. *Renew. Energy* **2022**, *188*, 450–464. [CrossRef]
17. Mori, Y.; Hijikata, K.; Himeno, N.; Nakayama, W. Fundamental research on heat transfer performances of solar focusing and tracking collector. *Sol. Energy* **1977**, *19*, 595–600. [CrossRef]
18. Mosleh, H.J.; Mamouri, S.J.; Shafii, M.B.; Sima, A.H. A new desalination system using a combination of heat pipe, evacuated tube and parabolic trough collector. *Energy Convers. Manag.* **2015**, *99*, 141–150. [CrossRef]
19. Nešović, A.; Lukić, N.; Taranović, D.; Nikolić, N. Theoretical and experimental investigation of the glass tube solar collector with inclined NS axis and relative EW single-axis tracking flat absorber. *Appl. Therm. Eng.* **2024**, *236*, 121842. [CrossRef]
20. Hayek, M.; Assaf, J.; Lteif, W. Experimental investigation of the performance of evacuated-tube solar collectors under eastern mediterranean climatic conditions. *Energy Procedia* **2011**, *6*, 618–626. [CrossRef]
21. Kaya, H.; Arslan, K. Numerical investigation of efficiency and economic analysis of an evacuated U-tube solar collector with different nanofluids. *Heat Mass Transf.* **2019**, *55*, 581–593. [CrossRef]
22. Liang, R.; Ma, L.; Zhang, J.; Zhao, D. Theoretical and experimental investigation of the filled-type evacuated tube solar collector with U tube. *Sol. Energy* **2011**, *85*, 1735–1744. [CrossRef]
23. Ditta, A.; Tabish, A.N.; Mujtaba, M.A.; Amjad, M.; Yusuf, A.A.; Chaudhary, G.Q.; Kalam, M.A. Experimental investigation of a hybrid configuration of solar thermal collectors and desiccant indirect evaporative cooling system. *Front. Energy Res.* **2022**, *10*, 979942. [CrossRef]
24. Kurhe, N.; Pathak, A.; Deshpande, K.; Jadkar, S. Compound parabolic solar collector–performance evaluation as per standard test method and actual field conditions for industrial process heat application in Indian context. *Energy Sustain. Dev.* **2020**, *57*, 98–108. [CrossRef]
25. Supankanok, R.; Sriwong, S.; Ponpo, P.; Wu, W.; Chandra-Ambhorn, W.; Anantpinijwatna, A. Modification of a solar thermal collector to promote heat transfer inside an evacuated tube solar thermal absorber. *Appl. Sci.* **2021**, *11*, 4100. [CrossRef]
26. Alqaed, S.; Mustafa, J.; Almehmadi, F.A.; Alharthi, M.A.; Sharifpur, M.; Cheraghian, G. Investigating the Effect of Tube Diameter on the Performance of a Hybrid Photovoltaic–Thermal System Based on Phase Change Materials and Nanofluids. *Materials* **2022**, *15*, 7613. [CrossRef]
27. Chai, S.; Yao, J.; Liang, J.D.; Chiang, Y.C.; Zhao, Y.; Chen, S.L.; Dai, Y. Heat transfer analysis and thermal performance investigation on an evacuated tube solar collector with inner concentrating by reflective coating. *Sol. Energy* **2021**, *220*, 175–186. [CrossRef]
28. Ma, L.; Lu, Z.; Zhang, J.; Liang, R. Thermal performance analysis of the glass evacuated tube solar collector with U-tube. *Build. Environ.* **2010**, *45*, 1959–1967. [CrossRef]
29. Chopra, K.; Tyagi, V.V.; Pandey, A.K.; Sari, A. Global advancement on experimental and thermal analysis of evacuated tube collector with and without heat pipe systems and possible applications. *Appl. Energy* **2018**, *228*, 351–389. [CrossRef]
30. Sulaiman, N.; Ihsan, S.I.; Bakar, S.N.S.A.; Majid, Z.A.A.; Zakaria, Z.A. Evacuated tubes solar air collectors: A review on design configurations, simulation works and applications. *Prog. Energy Environ.* **2023**, *25*, 10–32. [CrossRef]
31. Nešović, A.M.; Lukić, N.S.; Josijević, M.M.; Jurišević, N.M.; Nikolić, N.N. Novel flat-plate solar collector with an inclined NS axis and relative EW tracking absorbers and the numerical analysis of its potentials. *Therm. Sci.* **2024**, *28*, 2905–2916. [CrossRef]
32. Nešović, A.; Kowalik, R.; Bojović, M.; Janaszek, A.; Adamczak, S. Elevational Earth-Sheltered Buildings with Horizontal Overhang Photovoltaic-Integrated Panels—New Energy-Plus Building Concept in the Territory of Serbia. *Energies* **2024**, *17*, 2100. [CrossRef]
33. Janaszek, A.; Silva, A.F.d.; Jurišević, N.; Kanuchova, M.; Kozáková, Ľ.; Kowalik, R. The Assessment of Sewage Sludge Utilization in Closed-Loop Economy from an Environmental Perspective. *Water* **2024**, *16*, 383. [CrossRef]
34. Porowski, R.; Kowalik, R.; Grzmiączka, M.; Jurišević, N.; Gawdzik, J. Influence of initial temperature on laminar burning velocity in hydrogen-air mixtures as potential for green energy carrier. *Int. Commun. Heat Mass Transf.* **2023**, *146*, 106861. [CrossRef]
35. EnergyPlus Software. Available online: https://energyplus.net (accessed on 20 January 2024).
36. Jinzhou Innovation Jiacheng Optoelectronics Technology. Available online: https://srla.shengbangdaquartz.com (accessed on 12 April 2024).
37. Huang, X.; Wang, Q.; Yang, H.; Zhong, S.; Jiao, D.; Zhang, K.; Li, M.; Pei, G. Theoretical and experimental studies of impacts of heat shields on heat pipe evacuated tube solar collector. *Renew. Energy* **2019**, *138*, 999–1009. [CrossRef]
38. Rajput, R.K. *Engineering Thermodynamics: A Computer Approach*, 3rd ed.; Jones & Bartlett Learning: Boston, MA, USA, 2010.

39. Rabl, A. *Active Solar Collectors and Their Applications*, 1st ed.; Oxford University Press: New York, NY, USA, 1985.
40. Stine, W.B.; Harrigan, R.W. *Solar Energy Fundamentals and Design: With Computer Applications*, 1st ed.; Wiley: New York, NY, USA, 1985.
41. Yazdanpanahi, J.; Sarhaddi, F.; Adeli, M.M. Experimental investigation of exergy efficiency of a solar photovoltaic thermal (PVT) water collector based on exergy losses. *Sol. Energy* **2015**, *118*, 197–208. [CrossRef]
42. Chauhan, R.; Singh, T.; Thakur, N.S.; Kumar, N.; Kumar, R.; Kumar, A. Heat transfer augmentation in solar thermal collectors using impinging air jets: A comprehensive review. *Renew. Sustain. Energy Rev.* **2018**, *82*, 3179–3190. [CrossRef]
43. Hawwash, A.A.; Rahman, A.K.A.; Nada, S.A.; Ookawara, S. Numerical investigation and experimental verification of performance enhancement of flat plate solar collector using nanofluids. *Appl. Therm. Eng.* **2018**, *130*, 363–374. [CrossRef]
44. Kim, H.; Ham, J.; Park, C.; Cho, H. Theoretical investigation of the efficiency of a U-tube solar collector using various nanofluids. *Energy* **2016**, *94*, 497–507. [CrossRef]
45. DeWinter, F. *Solar Collectors, Energy Storage, and Materials*, 1st ed.; MIT Press: Cambridge, MA, USA, 1991.
46. Nešović, A. Theoretical model of solar incident angle for an optionally oriented fixed flat surface. *Tehnika* **2022**, *77*, 328–333. [CrossRef]
47. Dean, M. Multi-criteria analysis. *Adv. Transp. Policy Plan.* **2020**, *6*, 165–224.
48. Mitra, S.; Goswami, S.S. Application of simple average weighting optimization method in the selection of best desktop computer model. *Adv. J. Grad. Res.* **2019**, *6*, 60–68. [CrossRef]
49. Kumar, A.; Sah, B.; Singh, A.R.; Deng, Y.; He, X.; Kumar, P.; Bansal, R.C. A review of multi criteria decision making (MCDM) towards sustainable renewable energy development. *Renew. Sustain. Energy Rev.* **2017**, *69*, 596–609. [CrossRef]
50. Ministry of Construction Transport and Infrastructure. Rulebook of energy efficiency. Available online: https://www.mgsi.gov.rs (accessed on 4 March 2024).
51. Recycling Today. Available online: https://www.recyclingtoday.com (accessed on 5 June 2024).
52. Ramesh, T.; Prakash, R.; Shukla, K.K. Life cycle approach in evaluating energy performance of residential buildings in Indian context. *Energy Build.* **2012**, *54*, 259–265. [CrossRef]
53. Orman, Ł.J.; Chatys, R. Heat transfer augmentation possibility for vehicle heat exchangers. In Proceedings of the 15th International Conference "Transport Means", Kaunas, Lithuania, 20–21 October 2011; pp. 9–12.
54. Orman, Ł.J. Boiling heat transfer on single phosphor bronze and copper mesh microstructures. *EPJ Web Conf.* **2014**, *67*, 02087. [CrossRef]
55. Kalogirou, S. Thermal performance, economic and environmental life cycle analysis of thermosiphon solar water heaters. *Sol. Energy* **2009**, *83*, 39–48. [CrossRef]